Environmental Pollution 306 (2022) 119451

Contents lists available at ScienceDirect

Environmental Pollution

journal homepage: www.elsevier.com/locate/envpol

Interplay between arsenic and selenium biomineralization in *Shewanella* sp. O23S☆

Lucian C. Staicu [a,*], Paulina J. Wójtowicz [a], Zsombor Molnár [b,e], Encarnación Ruiz-Agudo [c], José Luis R. Gallego [d], Diego Baragaño [d], Mihály Pósfai [b,e]

[a] Faculty of Biology, University of Warsaw, Miecznikowa 1, 02-096, Warsaw, Poland
[b] Research Institute of Biomolecular and Chemical Engineering, University of Pannonia, Egyetem u. 10, H-8200, Veszprém, Hungary
[c] Department of Mineralogy and Petrology, University of Granada, Granada, Spain
[d] Environmental Biogeochemistry & Raw Materials Group and INDUROT, Campus de Mieres, University of Oviedo, C/Gonzalo Gutiérrez Quirós. S/N, 33600, Mieres, Spain
[e] ELKH-PE Environmental Mineralogy Research Group, University of Pannonia, Egyetem u. 10, H-8200, Veszprém, Hungary

ARTICLE INFO

Keywords:
Shewanella
Arsenic
Selenium
Biominerals
Environmental pollution

ABSTRACT

Bacteria play crucial roles in the biogeochemical cycle of arsenic (As) and selenium (Se) as these elements are metabolized via detoxification, energy generation (anaerobic respiration) and biosynthesis (e.g. selenocysteine) strategies. To date, arsenic and selenium biomineralization in bacteria were studied separately. In this study, the anaerobic metabolism of As and Se in *Shewanella* sp. O23S was investigated separately and mixed, with an emphasis put on the biomineralization products of this process. Multiple analytical techniques including ICP-MS, TEM-EDS, XRD, Micro-Raman, spectrophotometry and surface charge (zeta potential) were employed. *Shewanella* sp. O23S is capable of reducing selenate (SeO_4^{2-}) and selenite (SeO_3^{2-}) to red Se(-S)^0, and arsenate (AsO_4^{3-}) to arsenite (AsO_3^{3-}). The release of H_2S from cysteine led to the precipitation of AsS minerals: nanorod AsS and granular As_2S_3. When As and Se oxyanions were mixed, both As–S and Se(-S)^0 biominerals were synthesized. All biominerals were extracellular, amorphous and presented a negative surface charge (−24 to −38 mV). Kinetic analysis indicated the following reduction yields: SeO_3^{2-} (90%), AsO_4^{3-} (60%), and SeO_4^{2-} (<10%). The mix of SeO_3^{2-} with AsO_4^{3-} led to a decrease in As removal to 30%, while Se reduction yield was unaffected (88%). Interestingly, SeO_4^{2-} incubated with AsO_4^{3-} boosted the Se removal (71%). The exclusive extracellular formation of As and Se biominerals might indicate an extracellular respiratory process characteristic of various *Shewanella* species and strains. This is the first study documenting a complex interplay between As and Se oxyanions: selenite decreased arsenate reduction, whereas arsenate stimulated selenate reduction. Further investigation needs to clarify whether *Shewanella* sp. O23S employs multi-substrate respiratory enzymes or separate, high affinity enzymes for As and Se oxyanion respiration.

1. Introduction

Selenium (Se) and arsenic (As) are among the latest chemical elements identified as terminal electron acceptors used in bacterial and archaeal anaerobic respiration (Stolz and Oremland, 1999; Stolz et al., 2006; Staicu and Barton, 2021). Anaerobic respiration is an electrochemical process that couples the oxidation of an electron donor with the reduction of an electron acceptor, releasing electrons. This flow of electrons generates cellular energy by travelling via a protein-complex circuit (Canfield et al., 2005). A number of bacteria and archaea employ the oxyanions of Se, selenate (SeO_4^{2-}) and selenite (SeO_3^{2-}), and As, arsenate (AsO_4^{3-}) as terminal electron acceptors (Stolz et al., 2006). The main product of SeO_4^{2-} and SeO_3^{2-} respiration is elemental Se (Se^0), whereas the product of AsO_4^{2-} respiration is arsenite (AsO_3^{2-}) (Staicu and Barton, 2021). In the presence of sulfides (such as H_2S resulted from cysteine degradation), arsenite forms sulfur-bearing biominerals.

With regards to the energy yield, selenate produces twice the amount of energy (Gibbs free energy/ΔG^0) than arsenate, using lactate as an electron donor (Eqs. (1) and (2)) (Oremland et al., 1994; Newman et al., 1997). SeO_3^{2-}, although marginally reported as a microbial respiratory

☆ This paper has been recommended for acceptance by: Jörg Rinklebe
* Corresponding author.
E-mail address: staicu@biol.uw.edu.pl (L.C. Staicu).

https://doi.org/10.1016/j.envpol.2022.119451
Received 7 February 2022; Received in revised form 4 May 2022; Accepted 7 May 2022
Available online 12 May 2022

substrate, is the most energy-dense (Eq. (3)) of the three oxyanions listed above.

$$2SeO_4^{2-} + C_3H_5O_3^- \rightarrow 2SeO_3^{-2} + C_2H_3O_2^- + HCO_3^- + H^+ \quad \Delta G^0 = -343.1 kJ/mol\ lactate\left(C_3H_5O_3^-\right) \quad (1)$$

$$2SeO_4^{3-} + C_3H_5O_3^- + 4H^+ \rightarrow 2H_2AsO_3^- + C_2H_3O_2^- + CO_2 + 3H_2O \quad \Delta G^0 = -172\ kJ/mol\ lactate\left(C_3H_5O_3^-\right) \quad (2)$$

$$SeO_3^{2-} + C_3H_5O_3^- + H^+ \rightarrow Se^0 + C_2H_3O_2^- + HCO_3^- + 2H_2O \quad \Delta G^0 = -529.5\ kJ/mol\ lactate\left(C_3H_5O_3^-\right) \quad (3)$$

Due to their toxicity and mobility, As and Se pose environmental and human health problems (Stolz and Oremland, 1999). Selenium poisoning (by generating reactive oxygen species and dysfunctional molecules due to sulfur substitution) was recorded in various species of fish (Lemly, 2004) and aquatic birds (Ohlendorf et al., 2020). Arsenic is a metabolic poison (reacting with thiol groups and substituting for phosphorus) that affects drinking water quality in vast regions of Asia and South America (Podgorski and Berg, 2020). Apart from the natural contribution by arsenic-rich geothermal fluids, past (e.g. Cornwall, UK) and present (e.g. gold mining in Ashanti region, Ghana) mining activities, and coal combustion for energy production are significant sources of environmental pollution with arsenic (Podgorski and Berg, 2020; Baragaño et al., 2020; Staicu et al., 2021a). A vast contribution of selenium reaching the environment comes from anthropogenic activities, such as metal extraction and processing, coal combustion and agriculture practiced on seleniferous soils (Cordoba and Staicu, 2018; González-Fernández et al., 2018; Ohlendorf et al., 2020; Staicu et al., 2020a). The biomineralization process of Se and As oxyanions is essential for the precipitation their soluble and toxic forms to less/non-toxic biominerals (Staicu and Barton, 2021). Therefore, a better understanding of the biogeochemical interplay of these elements is essential to mitigate their environmental impact and to envision in- and ex-situ treatment solutions (e.g. bioremediation using selenium- and arsenic-respiring bacteria such as *Shewanella* sp. O23S).

To date, arsenic and selenium microbial biomineralization were treated separately, although several phylogenetically-diverse bacteria (e.g. *Bacillus arseniciselenatis* E1H, *B. selenatarsenatis* SF-1, *Sulfospirillum barnesii* SES-3) possess respiratory enzymes capable of harvesting energy from selenate, selenite and arsenate via anaerobic respiration. This enzymatic multi-substrate repertoire opens the discussion about the evolutionary and biogeochemical implications of ancient chemical systems predating aerobic respiration, and the biotechnological applications arising from this process (Staicu and Barton, 2021).

This paper presents a detailed study on As and Se bacterial biomineralization using *Shewanella* sp. O23S, investigating for the first time the metabolism of the two elements mixed in the same system. Cysteine utilization as a source of H_2S was based on a previous study using the same inoculum (Staicu et al., 2021a), as well as using previous studies on the cysteine-driven formation of AsS biominerals (Newman et al., 1997; Staicu et al., 2020b). The article also provides an in-depth mineralogical analysis of AsS and Se(-S)^0 biominerals produced by this bacterial strain. The biominerals were present exclusively in the extracellular environment and in the cellular vicinity, thus providing evidence about the co-respiration of the two elements. Mineralogical, kinetic and electron microscopy analyses were performed to test the hypothesis whether the two chemical elements can be biomineralized concomitantly - a situation occurring in natural and industrial (e.g. industrial wastewater) settings. The inhibition and stimulation outcomes that resulted from As and Se metabolic interplay might suggest a complex enzymatic system used by *Shewanella* sp. O23S to harvest cellular energy and/or detoxify As and Se oxyanions. In addition, the article provides information on the phase transition (amorphous to crystalline), localization, size (polydispersity) and morphology of the biogenic As- and Se-bearing particles.

2. Materials and methods

2.1. Bacterial inoculum

Bacterial strain *Shewanella* sp. O23S (hereinafter O23S) used in this study was isolated from a former gold mine in Złoty Stok (SW Poland) (Drewniak et al., 2015). To prepare the bacterial starter, a glycerol stocks sample was plated on Lysogeny broth (LB) agar (BioMaxima, Poland) and incubated aerobically overnight at 28 °C. Next, single colonies were picked and incubated aerobically under constant shaking in LB broth overnight (BioMaxima, Poland) at 28 °C and 150 rpm. 1% bacterial culture was used to inoculate every biotic incubation. In parallel, abiotic incubations were performed.

2.2. Reagents

Sodium selenate (Na_2SeO_4, 98.0%, from Acros), sodium selenite (Na_2SeO_3, 98.0%, from VWR), and sodium arsenate ($Na_2HAsO4*7H_2O$, ≥98.0%, from Thermo Scientific) were used without further purification. The stock solutions were filter-sterilized (0.2 μm polyethersulfone membrane syringe-driven filters, from VWR). Sodium lactate (as sodium L-lactate syrup, 60%) and yeast extract (YE) were purchased from Sigma. *L*-cysteine-HCl monohydrate (from VWR) was used as a source of H_2S. Pb-acetate test paper (Ref. 90744) was from Macherey-Nagel, Germany.

2.3. Growth media and incubations

Incubations were performed under anoxic conditions in Basal Mineral Media (BMM) containing (g L^{-1}): $Na_2HPO_4.2H_20$ (0.5), KH_2PO_4, (0.41), NH_4Cl (0.3), NaCl (0.3), $CaCl_2.2H_2O$ (0.11), $MgCl_2.6H_2O$ (0.1), $NaHCO_3$ (4), 1 mL L^{-1} acid trace element solution (without Se), 1 mL L^{-1} basic element solution (Stams et al., 1993), and 1 g L^{-1} YE. 1 mM $NaHAsO_4$, Na_2SeO_3 and Na_2SeO_4, 1 mM cysteine and 1 mM sodium lactate were amended to BMM in various combinations.

Vacuum filtration (Acrodisc®, pore size 0.2 μm) was used to sterilize the BMM solution. The incubations were performed in 500 mL serum bottles with butyl rubber septa and were closed with screw caps (Fig. S1). A 5-cm sterile Pb-acetate test paper was introduced in the headspace of each bottle before closing it. Next, the headspace was flushed with N_2 gas for 5 min using a 0.22 μm filter. The incubations were performed at 30 °C, pH ~7.5, for seven days, and without shaking (static conditions).

The incubation bottles were as follows: bottle A (positive control), bottle B (AsO_4^{3-}), bottle C (SeO_3^{2-}), bottle D (SeO_4^{2-}), bottle E (SeO_3^{2-} + AsO_4^{3-}), and bottle F (SeO_4^{2-} + AsO_4^{3-}).

2.4. Analytics

2.4.1. As and Se measurement

The samples were filter-sterilized and stored in sterile serum bottles at 4 °C until ICP analysis. Analysis was performed by Inductively Coupled Plasma Mass Spectrometry (ICP-MS 7700, Agilent Technologies, California, USA) using IDA (Isotopic Dilution Analysis) with a spike solution from ISC Science, Spain (Staicu et al., 2021a). High-purity standards (Charleston, SC, USA) were used for calibration. Detection limits were 1 μg L^{-1} for As and 2 μg L^{-1} for Se. To calculate As and Se removal (%) the following equation was used:

$$\text{removal}\ (\%) = \frac{C_0 - C_r}{C_0} * 100$$

where C_0 is the initial concentration and C_r is the residual concentration at a given sampling time (Staicu et al., 2017).

The pH was measured using a multi-parameter instrument (Prolab 4000, Schott, Jena, Germany).

The average and standard deviation values were used to present the results (three independent experiments, unless otherwise stated).

2.4.2. Electron microscopy

Transmission electron microscopy (TEM) was performed using a ThermoFisher Talos F200X electron microscope, operated at 200 kV accelerating voltage. Bright-field (BF) and high-resolution (HRTEM) images, as well as selected-area electron diffraction (SAED) were obtained in conventional TEM mode. In addition, images were obtained in scanning transmission (STEM) mode, using a high-angle annular dark-field (HAADF) detector. Energy-dispersive X-ray spectroscopy (EDS) was performed using a four-detector, built-in Super-X system. EDS elemental maps of selected regions were obtained in STEM mode, using ~200 pA current density and 10 s dwell time, and by collecting between 40 and 100 frames. Quantitative analyses of elemental compositions were performed on selected regions of the collected maps, after background subtraction and peak fitting, using the thin-film approximation (Molnár et al., 2021).

2.4.3. X-ray diffraction, Raman spectroscopy and zeta potential

Bacterial pellets and lead acetate strips were analyzed by X-Ray Diffraction (XRD) using an X'Pert PRO diffractometer (PANalytical): Cu Kα-radiation (λ = 1.5405 Å), 45 kV tension, 40 mA current, 3–70°2θ measurement range, 4 s per step, and 0.04°2θ step size. Diffraction patterns were analyzed using the computer code HighScore Plus 2.2.4 (PANalytical). Minerals were identified based on Powder Diffraction Standards (JCPDS) PDF-2 database. Lead acetate strips (neat and used in incubations) were directly stuck to the sample holder using C stubs, while bacterial pellets were crushed prior to XRD analysis (Staicu et al., 2021a).

Micro-Raman spectra from bacterial pellets were acquired with a HORIBA XploRa Plus microscope with a Peltier-cooled (213 K) CCD detector (1064 × 256 pixels) using a high power 532-nm diode laser in combination with a 2400 L/mm grating. The instrument was calibrated using a silicon wafer. The samples were analyzed using a 50 × objective in a direct-coupled microscope with enclosure. 10 s was used as sample exposure time (five accumulations), resulting in an adequate signal-to-noise ratio. LabSPEC6 Raman software was used to acquire spectra and were baseline-corrected using the OriginPro 8 software (Staicu et al., 2021a).

Zeta potential measurements were performed using a Zetasizer Nano ZS (Malvern Instrument Ltd., Worchestershire, UK) with a 633 nm laser beam and a scattering angle of 173° (at 25 °C) (Staicu et al., 2015a).

3. Results

3.1. Growth of Shewanella sp. O23S and biomineral formation

Fig. 1 presents the growth curve of O23S amended with As and Se oxyanions in various combinations (Fig. S1). The optical density (OD) of the growth control (bottle A) was time-dependent reaching a maximum value of ~1 after seven days of incubation. The highest optical density (~1.4) was recorded for the incubation containing SeO_3^{2-} (bottle C). Lower but similar OD values were measured for AsO_4^{3-} (bottle B), SeO_3^{2-} + AsO_4^{3-} (bottle E), and SeO_4^{2-} + AsO_4^{3-} (bottle F). The solutions started to change color after 24 h of incubation, bottles containing SeO_3^{2-} becoming red, while SeO_4^{2-} incubation producing a light pink color (Fig. S1). The bottle containing AsO_4^{3-} (B) started to develop a yellow color, indicative of orpiment (As_2S_3), formed by the reduction of AsO_4^{3-} to AsO_3^{3-} and the reaction of the latter with H_2S released from cysteine degradation. The intensity of colors increased with incubation time. Interestingly, bottles E (AsO_4^{3-} + SeO_3^{2-}) and F (AsO_4^{3-} + SeO_4^{2-}) produced an orange color. The pH of the solutions after 7 days of incubation was ~7.5 (±0.2).

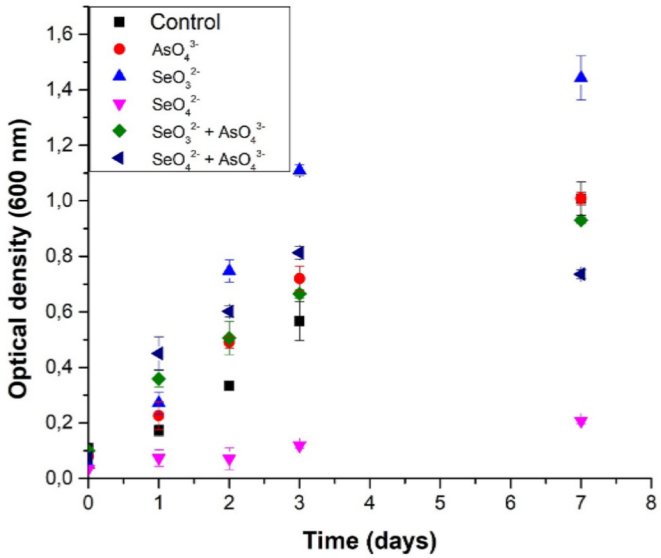

Fig. 1. Putative growth of *Shewanella* sp. O23S cultures in BMM amended with 1 mM cysteine, lactate and AsO_4^{3-}, SeO_4^{2-}, and SeO_3^{2-} (single and mixed).

3.2. As and Se oxyanions removal

The removal rates of the three oxyanions by O23S (single and mixed) are presented in Fig. 2. Although performed separately, the results of incubations containing AsO_4^{3-}, SeO_4^{2-}, and SeO_3^{2-} are all presented in Fig. 2a to facilitate a better comparison. Of the three, SeO_3^{2-} showed the highest removal yield (~90%) at day 7. AsO_4^{3-} removal scored second (~60%, day 7). In contrast, SeO_4^{2-} removal was limited (<10%) for the whole incubation time. Fig. 2b presents the removal of SeO_3^{2-} + AsO_4^{3-}. While the removal of SeO_3^{2-} stayed very close to the single-oxyanion incubation (~88%), AsO_4^{3-} removal displayed a significant decrease (~30%). More interestingly, SeO_4^{2-} + AsO_4^{3-} incubation produced a different outcome for the two oxyanions (Fig. 2c). While AsO_4^{3-} removal reached a maximum of ~30%, SeO_4^{2-} was pushed to an unprecedented 71% reduction. The abiotic controls did not lead to biomineral formation, nor did they contribute to As and Se removal.

3.3. As and Se (nano)particles

After 7 days of incubation, samples containing cell cultures and biominerals were collected and investigated by electron microscopy in terms of morphology of the bacterial cells and the morphology, structure and composition of precipitated solid materials. In the biotic control incubation (bottle A) no solid phase was observed (Fig. S3).

Fig. 3 presents the electron microscopy analysis of individual incubations containing AsO_4^{3-}, SeO_3^{2-} and SeO_4^{2-} (bottles B-D). The biomineralization products of AsO_4^{3-} incubation are presented in Fig. 3A–D. Arsenate reduction led to the production of two amorphous As- and S-bearing phases with different morphologies and varying As/S ratios (in the following: 'As–S particles'). Small (maximum 100 nm large in diameter), globular As–S particles could be seen attached to the surface of the bacterial cells (Fig. 3A). The elemental mapping identified As and S occurring together in the globular particles with As/S ratios varying between 0.5 and 0.65 (Fig. 3B), with the upper limit of the composition range being close to that of orpiment (As_2S_3). Another As–S phase forming few-μm-long nanorods was also identified, with an average As/S ratio between 0.95 and 1.04 (Fig. 3C), close to the composition of realgar (AsS). The networks of nanorods typically encompassed the cells, but also appeared detached from them. Again, the elemental maps suggested As and S were distributed homogeneously in the nanorods (Fig. 3D), and their structure appeared to be amorphous.

Fig. 3E (incubation with SeO_3^{2-}) shows extracellular globular Se

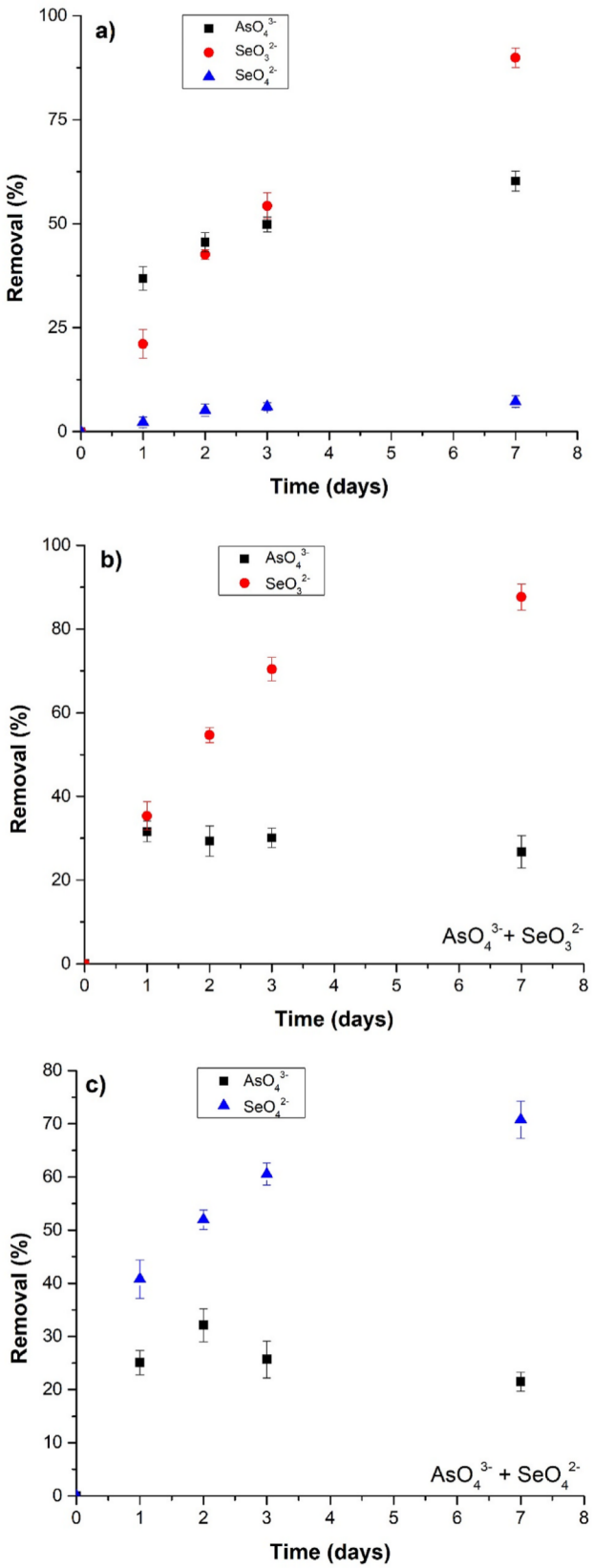

Fig. 2. As and Se removal by *Shewanella* in BMM. a) AsO_4^{3-}, SeO_4^{2-}, and SeO_3^{2-} removal as a function of incubation time. For easier understanding, the results are presented in the same panel, although the incubations were performed separately; b) AsO_4^{3-} + SeO_3^{2-} removal (mixed incubation); c) AsO_4^{3-} + SeO_4^{2-} removal (mixed incubation).

particles with minor S (in the following: 'Se(-S)^0 particles') attached to the surface or occurring in the immediate vicinity of the bacterial cells. The Se(-S)^0 particles were 100–200 nm large in diameter with uniform globular morphology and amorphous structure, and with Se/S ratios between 3.4 and 3.8 (Fig. 3F).

The SeO_4^{2-}-containing incubation generated similar globular Se(-S)^0 particles as in the case of SeO_3^{2-}, but the particles were less abundant and occurred with two distinct S contents (one set of particles with Se/S ratios between 3 and 4, and another with Se/S around 2). In addition, elongated aggregates of Se-containing particles with minor S were also present (Fig. 3G, F). Even though the various As–S and Se(-S)^0 phases had relatively distinct compositions, neither produced any reflections in the electron diffraction patterns, suggesting that their structures were essentially amorphous.

Fig. 4 presents results of the electron microscopy study of biominerals produced by the mixed incubations of As and Se oxyanions. AsO_4^{3-} + SeO_3^{2-} mix generated Se(-S)^0 particles having a high degree of similarity with the SeO_3^{2-}-only incubation (Fig. 4A). Beside (and attached to) the Se(-S)^0 particles (Fig. 4B), some amorphous Ca–P–O (probably Ca-phosphate) occurred on the surface of the cells (Fig. 4C). On the other hand, the presence of AsO_4^{3-} (AsO_4^{3-} + SeO_4^{2-}) had a marked impact on the biomineralization products (Fig. 4D–H). Se(-S)^0 particles had larger diameters (up to 500 nm) than in the case of the SeO_3^{2-}-only incubation, some displaying an elongated, filamentous morphology (Fig. 4E). Interestingly, As–S aggregates of several hundreds of nm to below 1 μm in size occurred around the Se(-S)^0 particles (Fig. 4H); such particles being absent in the case of the AsO_4^{3-} + SeO_3^{2-} incubation. Apparently, the As–S phases appeared as cloudy aggregates of nanoparticles, closely related to the globular Se(-S)^0 particles, and both phases typically appeared on the surfaces of the bacterial cells. Both the globular Se(-S)^0 particles and As–S aggregates showed large chemical variability. The Se/S ratio varied strongly even within the same globular particle, whereas the As–S phase also had minor Se content (Fig. 4F–G and **S4**).

3.4. Bulk mineralogy

Fig. 5 presents the X-ray diffractograms of the bacterial pellets and precipitated solid phases from incubations B–F. XRD patterns of the AsO_4^{3-} incubation (sample B, Fig. 5a) show diffraction peaks corresponding to arsenolite (As_2O_3) and, in some replicates, orpiment (As_2S_3), riding on a large background suggesting the presence of amorphous materials as well. Bacterial pellets from incubations amended with SeO_3^{2-} (sample C, Fig. 5b), SeO_4^{2-} (sample D, Fig. 5c), AsO_4^{3-} + SeO_3^{2-} (sample E, Fig. 5d), and AsO_4^{3-} + SeO_3^{2-} (sample F, Fig. 5e) were amorphous in some of the replicates, while in others peaks corresponding to crystalline trigonal Se (samples C and D) and As_2O_3 (sample F) were found.

The degradation of cysteine was assessed using the Pb-acetate assay (paper strips added in the headspace of incubations). The paper strip darkens in contact with H_2S released from cysteine degradation, forming PbS. After 24 h of incubation, the Pb-acetate strips from bottles A, B and D turned black on their full length inside the headspace, while that of bottle F turned black only to around a third of its length (Fig. S1 and S2). The situation stayed the same for bottles C and E throughout the incubation, only the C strip showing limited darkening (Fig. S2). XRD patterns of lead acetate strips are presented in Fig. S5. Diffraction peaks matching those of unreacted lead acetate (ICDD code 00-054-0326) and lead sulfide (ICDD code 01-078-1058) were detected in all diffractograms.

Raman spectra of bacterial pellets from incubations with AsO_4^{3-} (sample B, Fig. 6a) showed a broad band centered at ~350 cm^{-1} corresponding to the symmetric stretching vibration of As_2S_3 structural units of poorly crystalline arsenic sulfide materials (Vermeulen et al., 2019). All pellets from incubations containing Se oxyanions (samples C–F, Fig. 6b–e) showed a strong peak at ~250 cm^{-1}, which can be deconvoluted into three bands located at ~234 cm^{-1} (Se chains

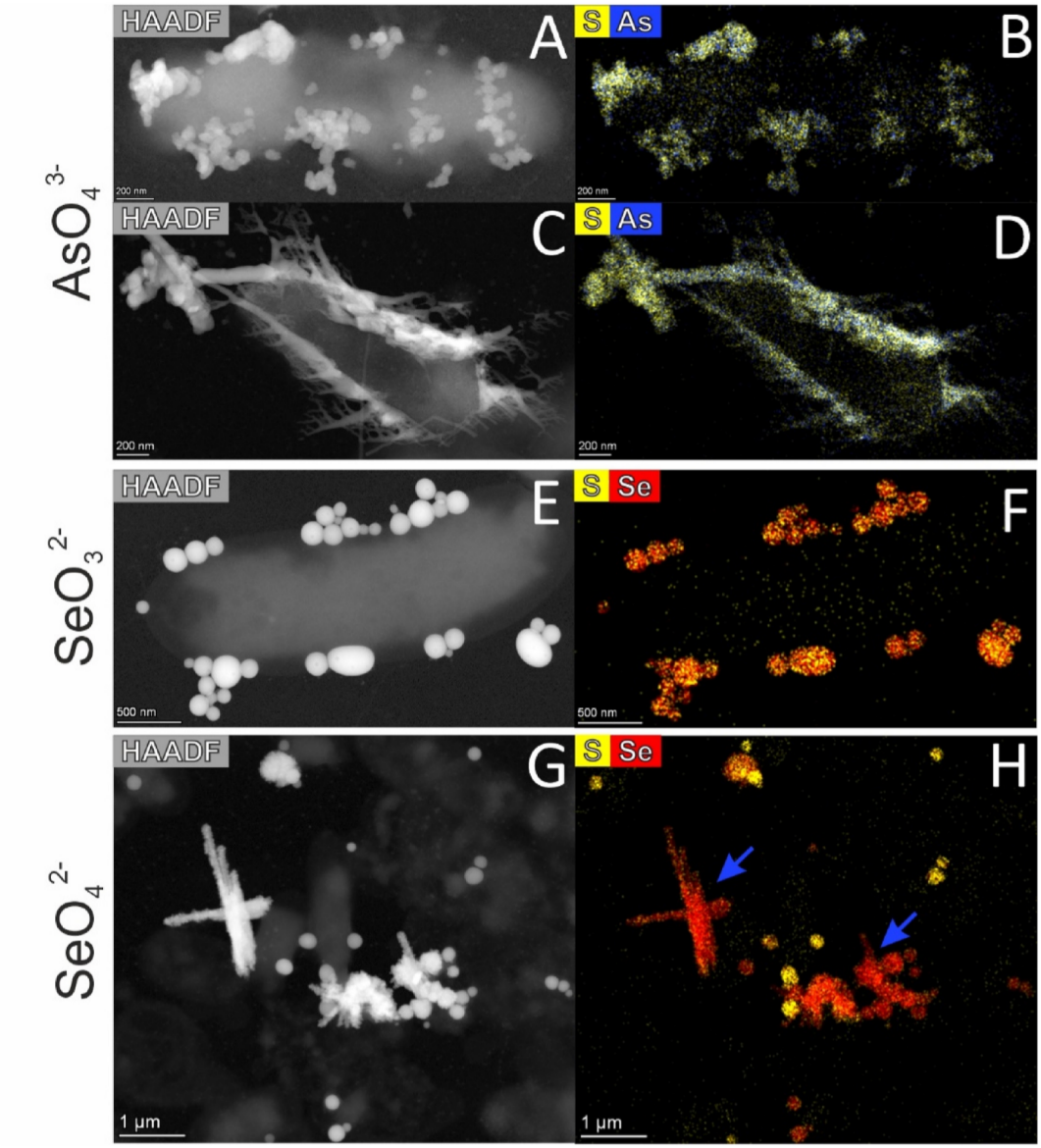

Fig. 3. STEM HAADF images (left panels) with the corresponding EDS elemental maps (right panels) obtained from bacterial cells and biomineralization products in growth media containing AsO_4^{3-} (A–D), SeO_3^{2-} (E–F), and SeO_4^{2-} (G–H). (A–B) Globular particles of As–S phases (with approximately As_2S_3 composition); (C–D) Network of As–S nanorods (with approximately AsS composition); (E–F) Uniformly globular Se nanoparticles with significant associated S content; (G–H) Aggregates of globular and lath-shaped particles of $Se(-S)^0$ (blue arrows) with minor and globular $Se(-S)^0$ particles with significant S content.

arranged in trigonal-like form), ~250 cm^{-1} (Se_n chains in disordered configurations), and ~260 cm^{-1} (Se_8 rings) (Yannopoulos and Andrikopoulos, 2004), revealing the presence of non-crystalline Se^0 in these samples. The samples showed a broad, weaker band at ~350 cm^{-1} that may be attributed to the vibration related to S–Se bond in As–S–Se materials (Han et al., 2013). Notably, this band was not observed in pellets from incubations with SeO_4^{2-} (sample D). Finally, samples incubated with AsO_4^{3-} + SeO_4^{2-}/SeO_3^{2-} (samples E and F) showed an additional band at ~460 cm^{-1} that corresponds to As–O stretching vibration in arsenic(III) oxide (Vermeulen et al., 2019), possibly arsenolite, according to our XRD results.

3.5. As and Se biominerals (summary)

The determined characteristics of the biominerals are summarized in Table 1. According to the electron micrographs, all biominerals produced by O23S were extracellular. Based on a comparison of TEM results with a visual observation of culture bottles, the yellow color of the AsO_4^{3-}-amended incubation was due to the presence of As–S biominerals, whereas the brick-red color of the SeO_3^{2-} incubation and the faint pink/brownish color of the SeO_4^{2-} incubation was caused by various types of $Se(-S)^0$ particles. When both As and Se oxyanions were present, the color after 7 days of incubation became orange, but showed a stratification with a reddish bottom layer and a top one of yellow appearance (Fig. S1). The biominerals occurred in different shapes, $Se(-S)^0$ being mainly globular, while As–S taking several morphologies: globular, nanorods and small aggregates. While electron diffraction suggested that the biomineral particles were all amorphous, XRD and Raman spectroscopy indicated the presence of minor crystalline phases, including Se^0 and orpiment (As_2S_3), in addition to arsenolite (As_2O_3) in some samples. Since aging of the material during transport and sample preparation may trigger the crystallization of amorphous phases, in Table 1 the observed biominerals are identified with their compositions instead of mineral names.

The cell-biomineral aggregates were also analyzed in terms of surface charge (zeta potential). The cell culture without As and Se

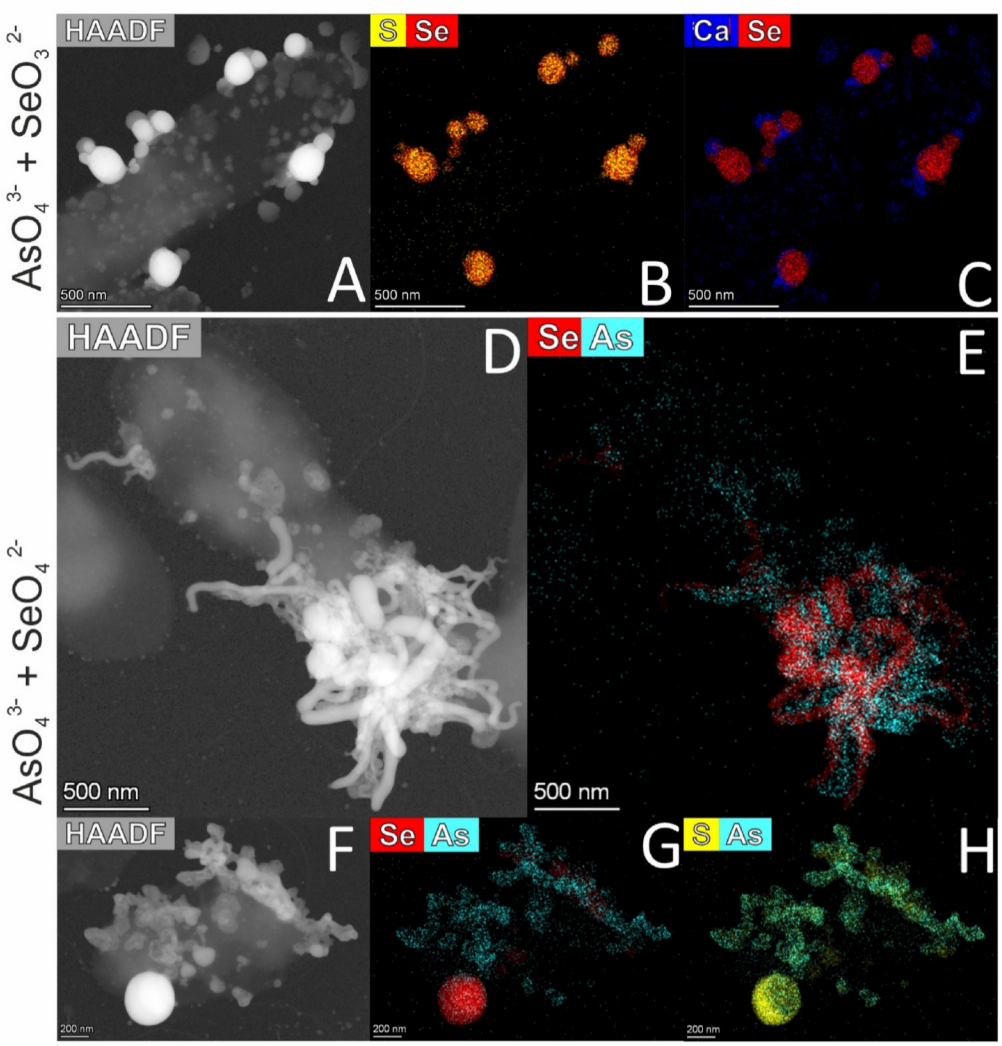

Fig. 4. STEM HAADF images with the corresponding EDS elemental maps, obtained from (A–C) AsO_4^{3-} + SeO_3^{2-} and (D–H) AsO_4^{3-} + SeO_4^{2-} incubations. (A) Globular Se(-S)^0 particles on the surface of a cell with associated amorphous Ca-phosphate; (D–E) Co-precipitation of cloudy aggregates of As–S particles with globular and elongated Se(-S)^0 on the surface of the cell; (F–H) Both globular Se(-S)^0 particles and aggregates of As–S have large chemical variability even within single particles (for further data see Fig. S4).

oxyanions had +0.1 mV, while the other incubations displayed the following values: AsO_4^{3-} (−35.2 mV), SeO_3^{2-} (−37.8 mV), SeO_4^{2-} (−23.7 mV), AsO_4^{3-} + SeO_3^{2-} (−34.8 mV), and AsO_4^{3-} + SeO_4^{2-} (−33.2 mV).

4. Discussion

4.1. As and Se metabolic interplay

Shewanella sp. O23S is a facultative anaerobe, able to respire using AsO_4^{3-}, $S_2O_3^{2-}$, NO_3^-, and Fe^{3+} as terminal electron acceptors; with lactate and citrate as electron donors (Drewniak et al., 2015). However, no study investigated as yet its capacity to grow in the presence of Se oxyanions, and As and Se oxyanions, accompanied by the production of biominerals.

While the formation of biominerals during growth phases makes the assessment of bacterial growth by optical density difficult to interpret, this method is nevertheless relevant to establish the biomineralization process induced by bacterial activity. The reduction of arsenate to arsenite, in the presence of H_2S released from cysteine, generates the yellow mineral As_2S_3 (orpiment) (Newman et al., 1997), while the reduction of SeO_4^{2-} and SeO_3^{2-} leads to the formation of red Se^0 (Staicu and Barton, 2021) (Fig. S1). Overall, the recorded OD values show a time-dependent increase, describing a typical bacterial growth curve (Fig. 1). The OD values follow the reduction rates of As and Se oxyanions (Fig. 2), with higher values for SeO_3^{2-}, AsO_4^{3-}, and the combination of arsenate with the two oxyanions of Se, while the growth on SeO_4^{2-} showed the lowest OD values. The growth of the strain using diverse substrates is indicative of its versatile metabolism, being capable of using both heterotrophic and anaerobic respiration strategies to sustain growth.

The removal yield of the oxyanions incubated separately for 7 days was as follows: SeO_3^{2-} (90%), AsO_4^{3-} (60%), SeO_4^{2-} (<10%) (Fig. 2a). In the absence of enzymatic and genetic data, the presence of detoxification or respiratory processes, or their mixed effects on the three oxyanions, cannot be established unambiguously. However, the biomineralization of As–S and Se(-S)^0, products of the reduction of As and Se oxyanions, was recorded exclusively in the extracellular milieu, providing an important piece of evidence in support of bacterial extracellular respiration (see detailed discussion below).

SeO_3^{2-} respiration is thermodynamically favorable and energy-dense (529 kJ/mol lactate, as per Eq. (3)), potentially explaining the highest removal yield among the three oxyanions. SeO_3^{2-} respiration was marginally described to date, the best characterized isolate being *Bacillus selenitireducens* strain MLS10 (Wells et al., 2019). Alternatively, SeO_3^{2-} reduction via detoxification cannot be ruled out. Detoxification of SeO_3^{2-} in bacteria is well established and documented in numerous publications but mainly under oxic conditions (Kessi et al., 1999; Ni et al., 2015; Staicu et al., 2015b; Piacenza et al., 2019).

In O23S, AsO_4^{3-} reduction might take place via respiration or detoxification since its genome was shown to carry genes for dissimilatory reduction (*arr* operon) and arsenic resistance (*ars* genes) (Uhrynowski et al., 2019). From a thermodynamic perspective, AsO_4^{3-}

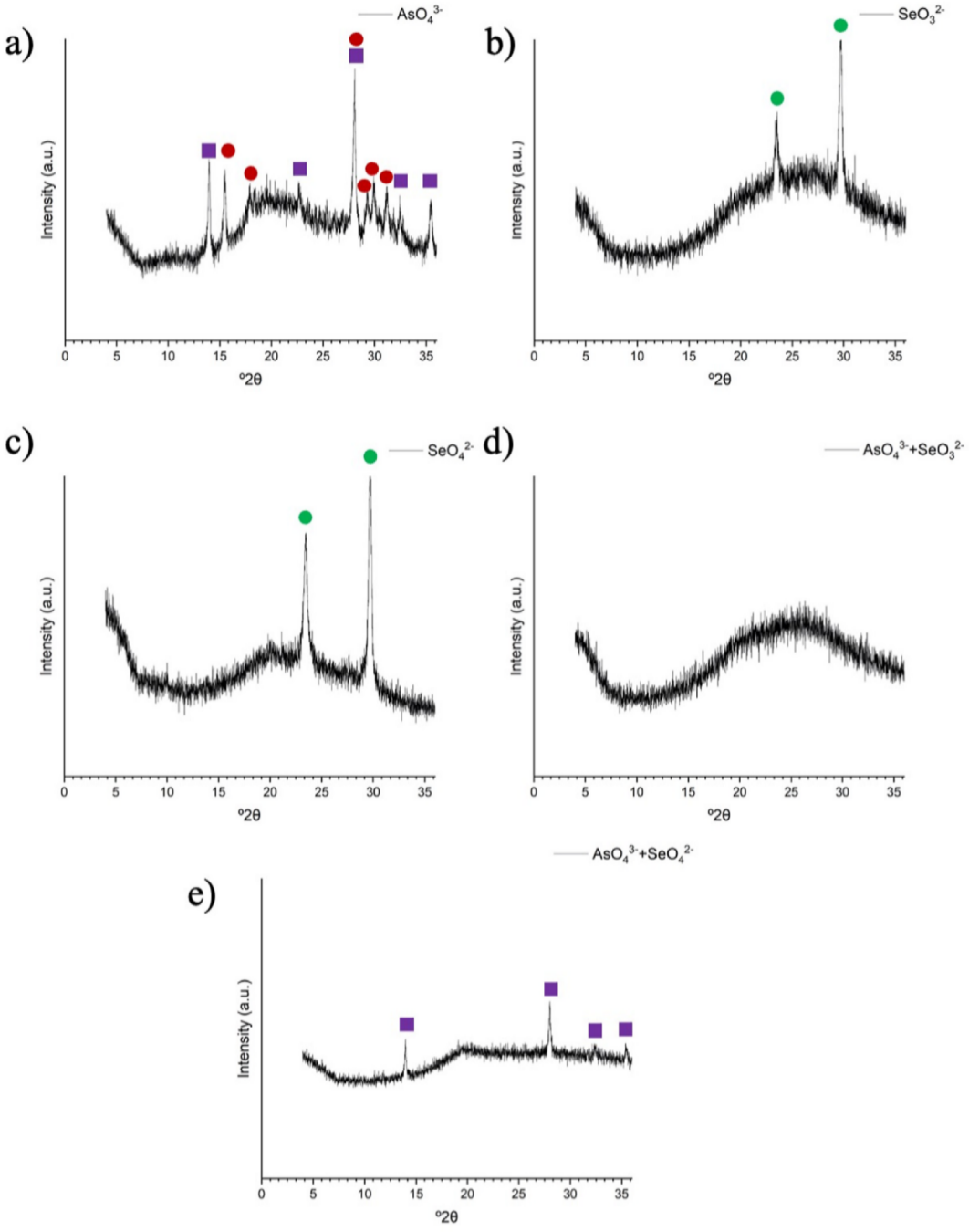

Fig. 5. XRD patterns of bacterial pellets from incubations amended with a) AsO_4^{3-}, b) SeO_3^{2-}, c) SeO_4^{2-}, d) AsO_4^{3-} + SeO_3^{2-}, and e) AsO_4^{3-} + SeO_4^{2-}. ■ diffraction peaks from arsenolite (As_2O_3); ● diffraction peaks from orpiment (As_2S_3); ● diffraction peaks from trigonal Se^0. The large hump between about 15 and 35° in all diffractograms indicates the presence of amorphous materials.

respiration provides sufficient energy to sustain growth (172 kJ/mol of lactate, as per Eq. (2)). As a comparison, the environmentally-ubiquitous respiration of SO_4^{2-} by sulfate-reducing bacteria (SRB) yields only ~50 kJ/mol of lactate (Barton and Fauque, 2009).

SeO_4^{2-} respiration (Eq. (1)) is well investigated (from thermodynamics to respiratory enzymes and genetic determinants) (the reader is referred to Staicu and Barton, 2021 for a full treatment on the topic). On the other hand, the mechanism involved in the (non-respiratory) reduction of SeO_4^{2-} in bacteria is unknown, selenate reduction being less prevalent than that of selenite. In general, it is considered that SeO_4^{2-} is less toxic than SeO_3^{2-} for bacteria (Stolz and Oremland, 1999; Fernández-Martínez and Charlet, 2009). In spite of the formation of a red color, indicative of Se^0, the reduction yield of SeO_4^{2-} (<10% after 7 days of incubation) could indicate a marginal detoxification reaction or a sub-optimal SeO_4^{2-} respiration.

The incubation of Se oxyanions with AsO_4^{3-} could provide further clues about the metabolic pathways of the two elements. The incubation of AsO_4^{3-} + SeO_3^{2-} resulted in a marked decrease in As removal (from 60% to 30%), while the Se removal yield was unaffected (from 90% to 88%) (Fig. 2b). This could indicate the thermodynamic advantage of using SeO_3^{2-} over AsO_4^{3-} (529 kJ/mol of lactate vs 172 kJ/mol of lactate). *Bacillus selenitireducens* MLS10 is the only bacterial isolate reported as yet to respire both AsO_4^{3-} (Afkar et al., 2003) and SeO_3^{2-} (Wells et al., 2019), but no competition study involving the two oxyanions has

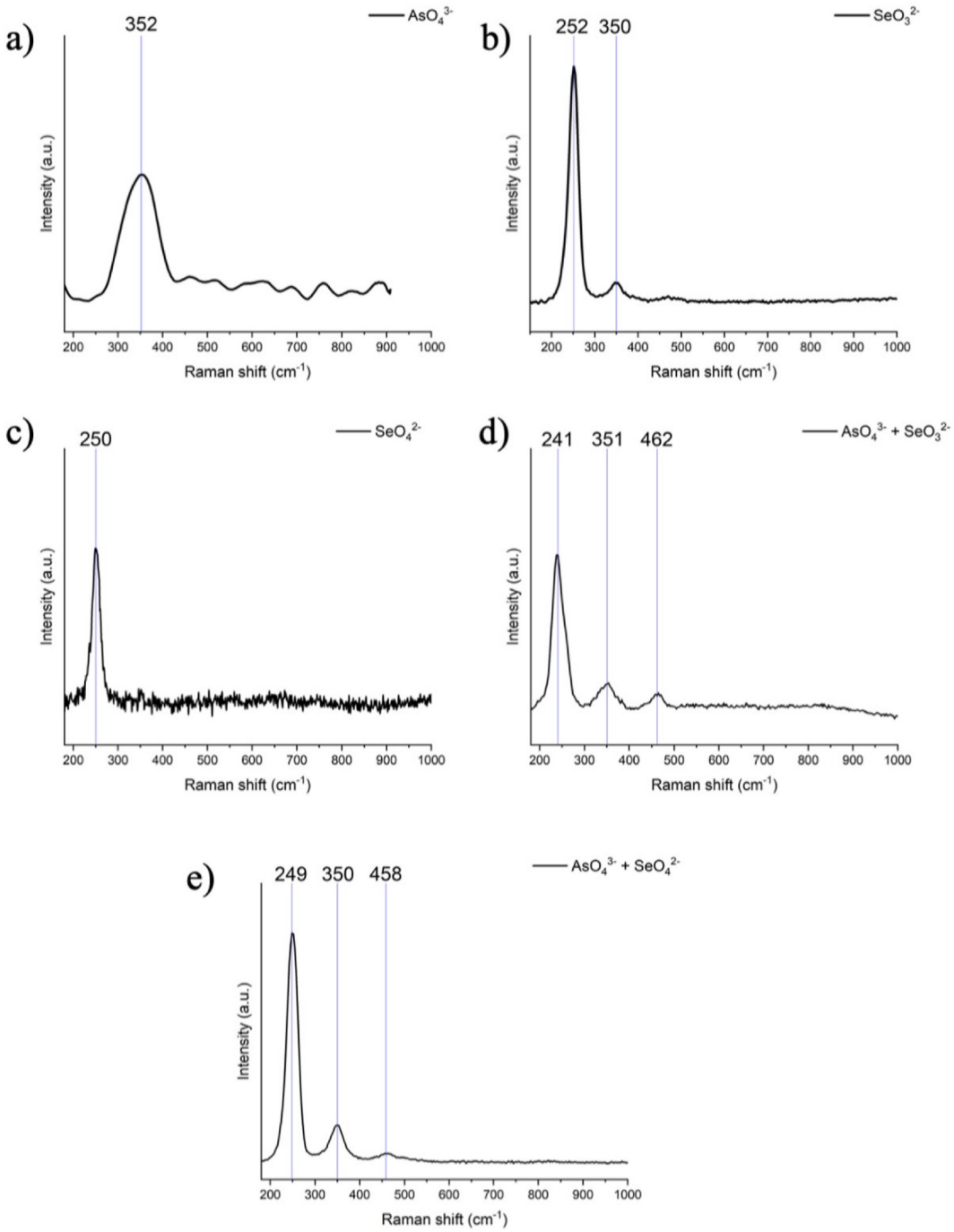

Fig. 6. Raman spectra of bacterial pellets from incubations amended with a) AsO_4^{3-}, b) SeO_3^{2-}, c) SeO_4^{2-}, d) AsO_4^{3-} + SeO_3^{2-}, and e) AsO_4^{3-} + SeO_4^{2-}.

been performed. Alternatively, the culture could have preferentially reduced SeO_3^{2-} to counteract its high toxicity. This, however, would not explain the decrease of AsO_4^{3-} removal yield since detoxification and anaerobic respiration are separate processes.

Interestingly, the most startling results came from the co-incubation of AsO_4^{3-} + SeO_4^{2-} (Fig. 2c). Whereas AsO_4^{3-} removal showed comparable results as in Fig. 2b (in the 25-30% range), SeO_4^{2-} removal unexpectedly rose to 71% (day 7), progressively with incubation time. A possible explanation could be the use of AsO_4^{3-} import channels for SeO_4^{2-} due to structural similarity between the two oxyanions.

Another explanation could be the presence of a multi-substrate respiratory reductase capable of utilizing both AsO_4^{3-} and SeO_4^{2-} as terminal electron acceptors. Several bacterial isolates such as *Sulfurospirillum barnesii* SES-3 (Phylum *Proteobacteria*), *Bacillus arseniciselenatis* E1H and *B. selenatarsenatis* SF-1 (Phylum *Firmicutes*) and *Desulfurispirillum indicum* S5 (Phylum *Crysiogenates*) have been shown to respire on both AsO_4^{3-} and SeO_4^{2-} (Staicu and Barton, 2021). So far, only the reductase of *Sulfurospirillum barnesii* SES-3 was characterized to a certain extent (K_m, V_{max}) and only with regards to SeO_4^{2-} (Oremland et al., 1999). The fact that this trait is present in phylogenetically-diverse bacteria might indicate a common evolutionary scenario where these oxyanions co-existed in the environment in concentrations significant enough to be used for energy conservation. Apart from its documented respiration using AsO_4^{3-} (Drewniak et al., 2015; Uhrynowski et al., 2019), O23S may also possess the capacity to respire SeO_3^{2-} and SeO_4^{2-}, and in a follow up study we plan to investigate this versatile metabolism

Table 1
Characteristics of As and Se biominerals produced by *Shewanella* sp. O23S.

Precursors	Biomineral/s	Color	Particle shape	Localization	Surface charge (mV)[a]
AsO_4^{3-}, cysteine	As_2S_3 AsS	Yellow	Globular, Nanorods	Extracellular	−35.2 (2.2)
SeO_3^{2-}, cysteine	$Se(-S)^0$	Red	Globular	Extracellular	−37.8 (2.7)
SeO_4^{2-}, cysteine	$Se(-S)^0$	Red	Globular, filaments	Extracellular	−23.7 (0.6)
AsO_4^{3-}, SeO_3^{2-}, cysteine	AsS $Se(-S)^0$	Orange	Globular, Nanorods	Extracellular	−34.8 (0.7)
AsO_4^{3-}, SeO_4^{2-}, cysteine	AsS $Se(-S)^0$	Orange	Globular, Aggregates	Extracellular	−33.2 (1.8)

The pH of the solutions (collected after 7 days of incubation) was ~7.5.
[a] the values in brackets represent the standard deviation of three measurements.

using molecular and bioinformatics techniques. O23S stands aside due to its capacity to reduce SeO_3^{2-} and SeO_4^{2-} to red Se^0 particles under both oxic and anoxic conditions (data unpublished).

4.2. Biominerals

$Se(-S)^0$ and As–S biominerals produced by O23S were extracellular (Figs. 3 and 4). This could suggest the presence of a respiratory process capable of depositing the by-products outside the bacterial cell. Extracellular respiration involves electron transfer to or from extracellular substrates, generating cellular energy (Gralnick and Newman, 2007). In addition, it provides the advantage of depositing solid by-products in the extracellular milieu. Numerous strains belonging to *Shewanella* genus are particularly known to possess this type of respiration (Gralnick et al., 2006; Marsili et al., 2008).

$Se(-S)^0$ particles synthesized by O23S are amorphous, have a globular shape and are polydisperse (<200 nm). Polydispersity in biogenic particles could indicate an Ostwald ripening process where smaller particles dissolve, while the larger ones increase in size as a function of incubation time. Biogenic $Se(-S)^0$ particles exhibit a negative surface charge (−37.8 mV for SeO_3^{2-}-sourced $Se(-S)^0$ and −23.7 mV for SeO_4^{2-}-sourced $Se(-S)^0$). In contrast, the cell culture unexposed to Se and As oxyanions has a +0.1 mV. This may indicate an active coating of Se^0 particles with a biopolymer layer. Previous studies have documented the colloidal stability of biogenic Se^0 linked with a biopolymer layer (Buchs et al., 2013; Staicu et al., 2015a). The association of sulfur (S) with biogenic Se^0 might be explained by the close chemical properties of the two elements (both are chalcogens and form similar structural elements, such as 8-membered, covalently bonded rings). These results are in agreement with Vogel et al. (2018), who identified $Se_{8-n}S_n$ spheres in *Azospirillum brasilense*. Since $Se(-S)^0$ particles were formed in both high (850 mg L^{-1}) and low (<300 mg L^{-1}) sulfate concentrations, the presence of S does not seem to play a decisive role in the biosynthesis of $Se(-S)^0$ particles.

In this study, As biomineralization produced amorphous As–S phases with compositions close to those of AsS (realgar) and As_2S_3 (orpiment), as observed by TEM; in addition, crystalline orpiment was detected by XRD (Fig. 5). Globular particles were mainly associated with close to As_2S_3 compositions, whereas filamentous biominerals were associated with compositions near AsS. Using an anaerobic biofilm mixed culture, Rodriguez-Freire et al. (2014) reported on the formation of orpiment and realgar by the reduction of AsO_4^{3-} and SO_4^{2-}, indicating pH as a potential factor for the formation of the two As–S mineral species (6.1–7.2 pH range), the proportion of orpiment increasing with pH. The pH change in our study was ~0.2, thus the influence of this parameter with regards to biomineral speciation could be considered negligible. Because the incubations were performed in the batch mode in serum bottles, redox potential dynamic could not have been recorded and used to refine the interpretation of the results. Arsenic sulfide (As–S) filaments (20–100 nm in diameter and 30 μm in length) were described in *Shewanella* sp. HN-41 using AsO_4^{3-} and $S_2O_3^{2-}$ as substrates (Lee et al., 2007). On the other hand, monodisperse, spherical, both intra- and extracellular As_2S_3 particles were identified under sulfate-reducing conditions, formed by the As-respiring bacterium *Desulfotomaculum auripigmentum* (Newman et al., 1997). In aggregate, these findings suggest that As–S biominerals are rather microbial species-specific, the pH and other parameters related to incubations conditions playing only a marginal role in their mineralogical identity. Additionally, the transition between different minerals and morphotypes could be one possible explanation for the diversity of As–S biominerals recorded so far.

The mix of arsenate with selenate and selenite resulted in systems with some characteristics significantly different from the case when the oxyanions were incubated separately (Table 1). AsO_4^{3-} + SeO_4^{2-} incubation showed Se particles with larger diameters (up to 500 nm) than in the case of SeO_3^{2-}-sourced $Se(-S)^0$, some displaying an elongated, filamentous morphology (Fig. 4E). Several-100-nm large aggregates of As–S surrounding $Se(-S)^0$ were recorded (Fig. 4H), such particles being absent in the case of AsO_4^{3-} + SeO_3^{2-} incubation. These results are in line with the visual observation that As and Se containing incubations led to an orange color, indicative of the formation of both $Se(-S)^0$ and As–S biominerals. In addition, both the globular $Se(-S)^0$ particles and As–S aggregates showed large chemical variability, suggesting a dynamic biomineralization process (Fig. S4).

Although the intracellular accumulation of biominerals has been reported in numerous publications (Weiner and Addadi, 2011; Pósfai et al., 2013; Qin et al., 2020; Ruiz-Fresneda et al., 2020; Cosmidis and Benzerara, 2022 etc.), all electron micrographs taken in this study revealed extracellular $Se(-S)^0$ and AsS biominerals surrounding structurally-undamaged bacterial cells. Previous studies have reported a pathway of nucleation (due to temporarily high concentrations of ions forming a disordered solid phase in intracellular membrane-bound vesicles), followed by the transport of these vesicles to the final biomineralization site (Weiner and Addadi, 2011). The use of intracellular membrane-bound vesicles has been shown for carbonate and magnetite biomineralization, but not for arsenic or selenium bacterial biominerals. A possible explanation for the extracellular biominerals reported in this study might be the ability of this strain of *Shewanella* to perform extracellular respiration, as it has been reported for other strains belonging to *Shewanella* genus (Gralnick et al., 2006; Marsili et al., 2008). Nevertheless, the biomineralization pathway of As and Se biominerals remains an open question, most notably the transition of Se from the red amorphous form to the trigonal polymorph.

It is important to mention the challenge of clearly establishing the mineralogy of biogenic minerals, taking into consideration the use of various analytical techniques and the effect of aging on samples. In our case, the aging effect appears to enhance the crystallinity of $Se(-S)^0$ and As–S biominerals (Fig. 5). Lee at al. (2007) documented the transition of biogenic As_2S_3 from amorphous toward polycrystalline phases of realgar and duranusite (As_4S), correlating it with changes in electrical and photoconductive properties. In the present study, while electron diffraction of freshly prepared samples suggested that all precipitates were amorphous, the XRD and Raman studies of pellets showed in some cases the presence of crystalline orpiment and trigonal Se^0 (Figs. 5 and 6).

4.3. Arsenic and selenium in the environment and in anthropogenic settings

Staicu et al. (2021b) investigated the bioremediation potential of O23S using a real polymetallic industrial effluent (resulted from gold mining activities). The effluent was dominated by As (~2300 μg L^{-1}), but also contained Co, Mo, Sb, Se, Zn (<250 μg L^{-1}) and around 1.6 g

L^{-1} of SO_4^{2-}. The incubation of the effluent with O23S (under anoxic conditions, 30 °C, pH 7, batch mode) containing cysteine, lactate and yeast extract led to variable removal yields of several elements: As (27%), Co (80%), Mo (78%), Se (88%), Sb (83%), and Zn (90%) (Staicu et al., 2021b). The removal of As and Se may have been via respiration, while, in the case of metals, the degradation of cysteine to H_2S could have contributed to their precipitation as metal sulfides.

The precipitation of As and Se as sulfides significantly decreases their toxicity and environmental impact because of the high stability of these minerals (Pósfai and Dunin-Borkowski, 2006; Park and Faivre, 2021). As such, the microbially-driven formation of metal sulfides may be considered an important source of natural attenuation of such pollutants present in brownfield and metal mining sites (Gallego et al., 2015; Di Lodovico et al., 2021). Additionally, the formation of sulfide-bearing biominerals in industrial effluents and mine-impacted streams may contribute to the recovery of mineral resources as an alternative to conventional energy-intensive and environmentally-degrading mining activities (Zhang et al., 2020; Abramov et al., 2021; Paganin et al., 2021; Staicu et al., 2021b). In a follow up study we plan to explore the capacity of O23S to recover metals as sulfides using industrial and natural polymetallic water samples. The investigation will be conducted in continuous mode of operation (bioreactors) paying attention to hydraulic retention time (HRT), redox potential and pH parameters, as well as the supplementation of the matrix with trace elements.

Understanding the biogeochemical interplay of As and Se plays an important role in envisioning solutions for cleaning up sites/industrial matrices (wastewater) polluted with the two elements. The formation of AsS and $Se(-S)^0$ biominerals is a critical step in the biogeochemical cycles of As and Se, as the mineral-bound elements exhibit decreased environmental mobility and toxicity to biota. Bacteria able to reduce both elements possess an advantage when used for treating a wider spectrum of pollutants.

5. Conclusions

- *Shewanella* sp. O23S displays an extended arsenic and selenium biomineralization repertoire under anoxic conditions by forming AsS minerals using AsO_4^{3-}: nanorod AsS and granular As_2S_3; and $Se(-S)^0$.
- $Se(-S)^0$ was formed by the reduction of both Se oxyanions, SeO_3^{2-} and SeO_4^{2-}, thus showing high Se reduction versatility.
- While inhibition (SeO_3^{2-} vs AsO_4^{3-}) and stimulation (AsO_4^{3-} vs SeO_4^{2-}) reactions are involved in the microbial transformation of these oxyanions, both As–S and $Se(-S)^0$ biominerals were formed when As and Se were mixed.
- Cysteine metabolism with the release of H_2S plays an essential role in the precipitation of As–S biominerals and might have a contribution to Se^0 formation.
- The extracellular formation of As–S and $Se(-S)^0$ biominerals might indicate a specialization of *Shewanella* for extracellular respiration, with the disposal of the biomineralization products to the extracellular milieu.
- All biominerals investigated in this study were amorphous, negatively-charged and a slight crystallization tendency was observed during the drying and storage of the biominerals for XRD and Micro-Raman analysis.
- This study provides evidence about the mixed microbial metabolism and biomineralization of As and Se and opens future research directions on the enzymatic systems and genetic determinants involved in this process with potential applications for bioremediation and resource recovery.

Author contribution

Lucian Staicu designed the experiments and wrote the manuscript; Paulina Wojtowicz performed the experiments and revised the manuscript; Zsombor Molnár performed the electron microscopy analysis and revised the manuscript; Encarnacion Ruiz-Agudo performed the mineralogical analysis and revised the manuscript; José Luis Gallego discussed the experiments and revised the manuscript; Diego Baragaño perfomed the ICP analysis and revised the manuscript; Mihály Pósfai discussed the experiments, supervised the electron microscopy analysis, and revised the manuscript.

Declaration of competing interest

The authors declare the following financial interests/personal relationships which may be considered as potential competing interests: Lucian Staicu reports financial support was provided by National Science Center (NCN).

Acknowledgements

LS and PW acknowledge the National Science Centre (NCN), Poland (grant 2017/26/D/NZ1/00408) for financial support. We would also like to thank the Environmental Assay Unit of the Scientific and Technical Services of the University of Oviedo (Spain) for their technical support. Diego Baragaño would like to thank the European Union-NextGeneration EU, Ministerio de Universidades, and Plan de Recuperación, Transformación y Resiliencia, through a call of the Universidad de Oviedo for the Postdoctoral grant (Ref. MU-21-UP2021-030 32892642). ERA acknowledges funding by the Spanish Government (grants RTI2018-099565-B-I00 and PCI2019-111927-2), the Junta de Andalucía (research group RNM-179), and the University of Granada (Unidad Científica de Excelencia UCE-PP2016-05). MP and ZM acknowledge support from the National Research, Development and Innovation Office (Hungary) (grant NKFIH-471-3/202). The authors acknowledge Federica Clincenaru for designing the graphical abstract.

Appendix A. Supplementary data

Supplementary data to this article can be found online at https://doi.org/10.1016/j.envpol.2022.119451.

References

Abramov, S.M., Straub, D., Tejada, J., et al., 2021. Biogeochemical niches of Fe-cycling communities influencing heavy metal transport along the Rio Tinto, Spain. Appl. Environ. Microbiol. 88 (4), e0229021 (AEM0229021).

Afkar, E., Lisak, J., Saltikov, C., Basu, P., Oremland, R.S., Stolz, J.F., 2003. The respiratory arsenate reductase from *Bacillus selenitireducens* strain MLS10. FEMS Microbiol. Lett. 226, 107–112.

Baragaño, D., Boente, C., Rodríguez-Valdés, E., Fernández-Braña, A., Jiménez, A., Gallego, J.L.R., González-Fernández, B., 2020. Arsenic release from pyrite ash waste over an active hydrogeological system and its effects on water quality. Environ. Sci. Pollut. Res. 27 (10), 10672–10684.

Barton, L.L., Fauque, G.D., 2009. Biochemistry, physiology and biotechnology of sulfate-reducing bacteria. Adv. Appl. Microbiol. 68, 41–98.

Buchs, B., Evangelou, M.W., Winkel, L.H., Lenz, M., 2013. Colloidal properties of nanoparticular biogenic selenium govern environmental fate and bioremediation effectiveness. Environ. Sci. Technol. 47 (5), 2401–2407.

Canfield, D.E., Kristensen, E., Thamdrup, B., 2005. Thermodynamics and microbial metabolism. In: Southward, A.J., Tyler, P.A., Young, C.M., Fuiman, L.A. (Eds.), Aquatic Geomicrobiology. Elsevier, Amsterdam, pp. 65–94.

Cordoba, P., Staicu, L.C., 2018. Flue Gas Desulfurization effluents: an unexploited selenium resource. Fuel 223, 268–276.

Cosmidis, J., Benzerara, K., 2022. Why do microbes make minerals? CR Geosci. 354, 1–39.

Di Lodovico, E., Marchand, L., Oustrière, N., Burges, A., et al., 2021. Potential ability of tobacco (*Nicotiana tabacum* L.) to phytomanage an urban brownfield soil. Environ. Sci. Pollut. Res. Int. 18, 1–18.

Drewniak, L., Stasiuk, R., Uhrynowski, W., Sklodowska, A., 2015. *Shewanella* sp. O23S as a driving agent of a system utilizing dissimilatory arsenate-reducing bacteria responsible for self-cleaning of water contaminated with arsenic. Int. J. Mol. Sci. 16, 14409-11427.

Fernández-Martínez, A., Charlet, L., 2009. Selenium environmental cycling and bioavailability: a structural chemist point of view. Rev. Environ. Sci. Biotechnol. 8, 81–110.

Gallego, J.R., Esquinas, N., Rodríguez-Valdés, E., Menéndez-Aguado, J.M., Sierra, C., 2015. Comprehensive waste characterization and organic pollution co-occurrence in a Hg and as mining and metallurgy brownfield. J. Hazard Mater. 300, 561–571.

González-Fernández, B., Rodríguez-Valdés, E., Boente, C., Menéndez-Casares, E., Fernández-Braña, A., Gallego, J.R., 2018. Long-term ongoing impact of arsenic contamination on the environmental compartments of a former mining-metallurgy area. Sci. Total Environ. 610–611, 820–830.

Gralnick, J.A., Vali, H., Lies, D.P., Newman, D.K., 2006. Extracellular respiration of dimethyl sulfoxide by *Shewanella oneidensis* strain MR-1. Proc. Natl. Acad. Sci. Unit. States Am. 103 (12), 4669–4674.

Gralnick, J.A., Newman, D.K., 2007. Extracellular respiration. Mol. Microbiol. 65, 1–11.

Han, X., Tao, H., Pan, R., Lang, Y., Shang, C., Xing, X., Tu, Q., Zhao, X., 2013. Structure and vibrational modes of As-S-Se glasses: Raman scattering and ab initio calculations. Phys. Procedia 48, 59–64.

Kessi, J., Ramuz, M., Wehrli, E., Spycher, M., Bachofen, R., 1999. Reduction of selenite and detoxification of elemental selenium by the phototrophic bacterium *Rhodospirillum rubrum*. Appl. Environ. Microbiol. 65, 4734–4740.

Lee, J.H., Kim, M.G., Yoo, B.Y., Myung, N.V., Maeng, J.S., Lee, T., Dohnalkova, A.C., Fredrickson, J.K., Sadowsky, M.J., Hur, H.G., 2007. Biogenic formation of photoactive arsenic-sulfide nanotubes by Shewanella sp strain HN-41. Proc. Natl. Acad. Sci. Unit. States Am. 104 (51), 20410–20415.

Lemly, A.D., 2004. Aquatic selenium pollution is a global environmental safety issue. Ecotoxicol. Environ. Saf. 59, 44–56. https://doi.org/10.1016/S0147-6513(03)00095-2.

Marsili, E., Baron, D.B., Shikhare, I.D., Coursolle, D., Gralnick, J.A., Bond, D.R., 2008. Shewanella secretes flavins that mediate extracellular electron transfer. Proc. Natl. Acad. Sci. Unit. States Am. 105 (10), 3968–3973.

Molnár, Z., Pekker, P., Dódony, I., Pósfai, M., 2021. Clay minerals affect calcium (magnesium) carbonate precipitation and aging. Earth Planet Sci. Lett. 567, 116971.

Newman, D.K., Kennedy, E.K., Coates, J.D., Ahmann, D., Ellis, D.J., Lovley, D.R., Morel, F.M., 1997. Dissimilatory arsenate and sulfate reduction in *Desulfotomaculum auripigmentum* sp. nov. Arch. Microbiol. 168, 380–388.

Ni, T.W., Staicu, L.C., Nemeth, R., Schwartz, C., Crawford, D., et al., 2015. Progress toward clonable inorganic nanoparticles. Nanoscale 7, 17320–17327.

Ohlendorf, H.M., Santolo, G.M., Byron, E.R., Eisert, M.A., 2020. Kesterson Reservoir: 30 years of selenium risk assessment and management. Environ. Manag. 16, 257–268.

Oremland, R.S., Switzer Blum, J., Culberston, C.W., Visscher, P.T., Miller, L.G., Dowdle, P., Strohmaier, F.E., 1994. Isolation, growth and metabolism of an obligately anaerobic, selenate-respiring bacterium, strain SES-3. Appl. Environ. Microbiol. 60, 3011–3019.

Oremland, R.S., Blum, J.S., Bindi, A.B., Dowdle, P.R., Herbel, M., Stolz, J.F., 1999. Simultaneous reduction of nitrate and selenate by cell suspensions of selenium-respiring bacteria. Appl. Environ. Microbiol. 65 (10), 4385–4392.

Paganin, P., Alisi, C., Dore, E., et al., 2021. Microbial diversity of bacteria involved in biomineralization processes in mine-impacted freshwaters. Front. Microbiol. 12, 778199.

Park, Y., Faivre, D., 2021. Diversity of Microbial Metal Sulfide Biomineralization. ChemPlusChem. https://doi.org/10.1002/cplu.202100457.

Piacenza, E., Presentato, A., Bardelli, M., Lampis, S., Vallini, G., Turner, R.J., 2019. Influence of bacterial physiology on processing of selenite, biogenesis of nanomaterials and their thermodynamic stability. Molecules 24 (14), 2532.

Podgorski, J., Berg, M., 2020. Global threat of arsenic in groundwater. Science 368, 845–850.

Pósfai, M., Dunin-Borkowski, R.E., 2006. Sulfides in biosystems. Rev. Mineral. Geochem. 61 (1), 679–714.

Pósfai, M., Lefèvre, C.T., Trubitsyn, D., Bazylinski, D.A., Frankel, R.B., 2013. Phylogenetic significance of composition and crystal morphology of magnetosome minerals. Front. Microbiol. 4, 344.

Qin, W., Wang, C.Y., Ma, Y.X., Shen, M.J., Li, J., Jiao, K., Tay, F.R., Niu, L.N., 2020. Microbe-mediated extracellular and intracellular mineralization: environmental, Industrial, and Biotechnological applications. Adv. Mater. 32 (22), e1907833.

Rodriguez-Freire, L., Sierra-Alvarez, R., Root, R., Chorover, J., Field, J.A., 2014. Biomineralization of arsenate to arsenic sulfides is greatly enhanced at mildly acidic conditions. Water Res. 66, 242–253.

Ruiz-Fresneda, M.A., Eswayah, A.S., Romero-González, M., Gardiner, P.H., Solari, P.L., Merroun, M.L., 2020. Chemical and structural characterization of Se^{IV} biotransformations by *Stenotrophomonas bentonitica* into Se^{0} nanostructures and volatiles Se species. Environ. Sci.: Nano 7 (7), 2140–2155.

Staicu, L.C., van Hullebusch, E.D., Oturan, M.A., Ackerson, C.J., Lens, P.N.L., 2015a. Removal of colloidal biogenic selenium from wastewater. Chemosphere 125, 130–138.

Staicu, L.C., Ackerson, C.J., Cornelis, P., Ye, L., Berendsen, R.L., et al., 2015b. *Pseudomonas moraviensis* subsp. stanleyae, a bacterial endophyte of hyperaccumulator *Stanleya pinnata*, is capable of efficient selenite reduction to elemental selenium under aerobic conditions. J. Appl. Microbiol. 119 (2), 400–410.

Staicu, L.C., Morin-Crini, N., Crini, G., 2017. Desulfurization: critical step towards enhanced selenium removal from industrial effluents. Chemosphere 117, 111–119.

Staicu, L.C., Bajda, T., Drewniak, L., Charlet, L., 2020a. Power generation: feedstock for high-value sulfate minerals. Minerals 10 (2), 188.

Staicu, L.C., Wojtowicz, P.J., Pósfai, M., Pekker, P., Gorecki, A., Jordan, F.L., Barton, L.L., 2020b. PbS biomineralization using cysteine: *Bacillus cereus* and the sulfur rush. FEMS Microbiol. Ecol. 96 (9) fiaa151.

Staicu, L.C., Barton, L.L., 2021. Selenium respiration in anaerobic bacteria: does energy generation pay off? J. Inorg. Biochem. 222, 111509.

Staicu, L.C., Wojtowicz, P.J., Bargano, D., Pósfai, M., Molnar, Z., Ruiz-Agudo, E., Gallego, J.L., 2021a. Bioremediation of a polymetallic, arsenic-dominated reverse osmosis reject stream. Lett. Appl. Microbiol. https://doi.org/10.1111/lam.13578.

Staicu, L.C., van Hullebusch, E.D., Ackerson, C.J., 2021b. Microbial Biominerals: toward new functions and resource recovery. Front. Microbiol. 12, 796374.

Stams, A.J.M., van Dijk, J.B., Dijkema, C., Plugge, C.M., 1993. Growth of syntrophic propionate-oxidizing bacteria with fumarate in the absence of methanogenic bacteria. Appl. Environ. Microbiol. 59, 1114–1119.

Stolz, J.F., Oremland, R.S., 1999. Bacterial respiration of arsenic and selenium. FEMS Microbiol. Rev. 23, 615–627.

Stolz, J.F., Basu, P., Santini, J.N., Oremland, R.S., 2006. Arsenic and selenium in microbial metabolism. Annu. Rev. Microbiol. 60, 107–130.

Uhrynowski, W., Radlinska, M., Drewniak, L., 2019. Genomic analysis of *Shewanella* sp. O23S - the natural host of the pSheB plasmid carrying genes for arsenic resistance and dissimilatory reduction. Int. J. Mol. Sci. 20, 1018.

Vermeulen, M., Palka, K., Vlček, M., Sanyova, J., 2019. Study of dry- and wet-process amorphous arsenic sulfides: synthesis, Raman reference spectra, and identification in historical art materials. J. Raman Spectrosc. 50, 396–406.

Vogel, M., Fischer, S., Maffert, A., Hübner, R., Scheinost, A.C., Franzen, C., Steudtner, R., 2018. Biotransformation and detoxification of selenite by microbial biogenesis of selenium-sulfur nanoparticles. J. Hazard Mater. 344, 749–757.

Weiner, S., Addadi, L., 2011. Crystallization pathways in biomineralization. Annu. Rev. Mater. Res. 41, 21–40.

Wells, M., McGarry, J., Gaye, M.M., Basu, P., Oremland, R.S., Stolz, J.F., 2019. Respiratory selenite reductase from *Bacillus selenitireducens* strain MLS10. J. Bacteriol. 201, e00614–e00618.

Yannopoulos, S.N., Andrikopoulos, K.S., 2004. Raman scattering study on structural and dynamical features of noncrystalline selenium. J. Chem. Phys. 121, 4747–4758.

Zhang, R., Hedrich, S., Römer, F., Goldmann, D., Schippers, A., 2020. Bioleaching of cobalt from Cu/Co-rich sulfidic mine tailings from the polymetallic Rammelsberg mine, Germany. Hydrometallurgy 197, 105443.

Supplementary file

Interplay between arsenic and selenium biomineralization in *Shewanella* sp. O23S

Lucian C. Staicu[1,*], Paulina J. Wojtowicz[1], Zsombor Molnár[2], Encarnacion Ruiz-Agudo[3], José Luis R. Gallego[4], Diego Baragaño[4], Mihály Pósfai[2]

[1]Faculty of Biology, University of Warsaw, Miecznikowa 1, 02-096 Warsaw, Poland

[2]Research Institute of Biomolecular and Chemical Engineering, University of Pannonia, Egyetem u. 10, H-8200, Veszprém, Hungary

[3]Department of Mineralogy and Petrology, University of Granada, Granada, Spain

[4]Environmental Biogeochemistry & Raw Materials Group and INDUROT, Campus de Mieres, University of Oviedo, C/Gonzalo Gutiérrez Quirós. S/N, 33600 Mieres, Spain

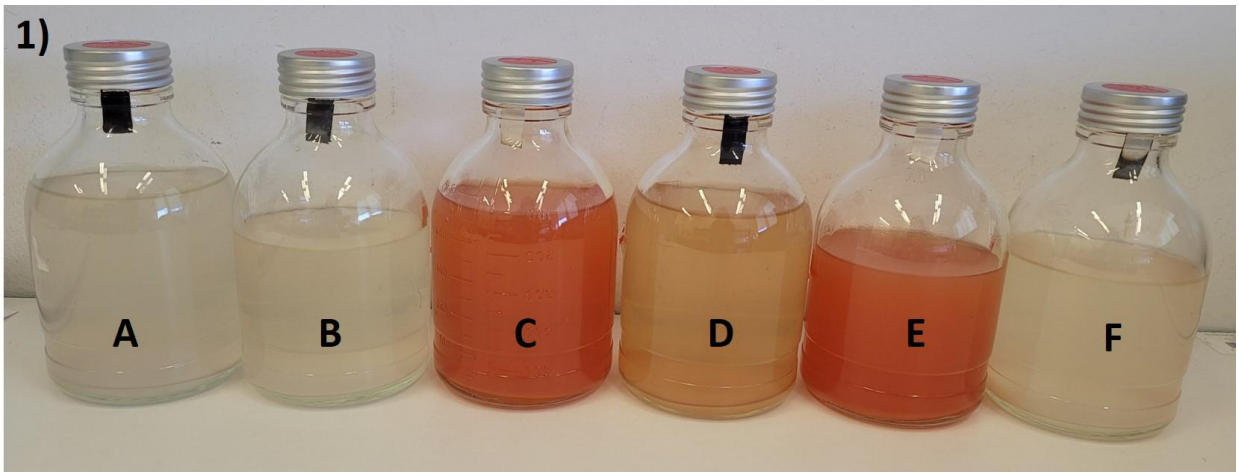
1)
A
B
C
D
E
F


2)
A
B
C
D
E
F


3)
A
B
C
D
E
F

Figure S1. Anaerobic incubations in BMM using *Shewanella* sp. O23S. A) BMM without As and Se oxyanions; B) 1 mM AsO_4^{3-}; C) 1 mM SeO_3^{2-}; D) 1 mM SeO_4^{2-}; E) 1 mM AsO_4^{3-} and 1 mM SeO_3^{2-}; F) 1 mM AsO_4^{3-} and 1 mM SeO_4^{2-}. Incubation time: 1) day 1; 2) day 2; 3) day 3; and 7) day 7. Growth conditions: 30 °C, pH ~7.5, dark, static.

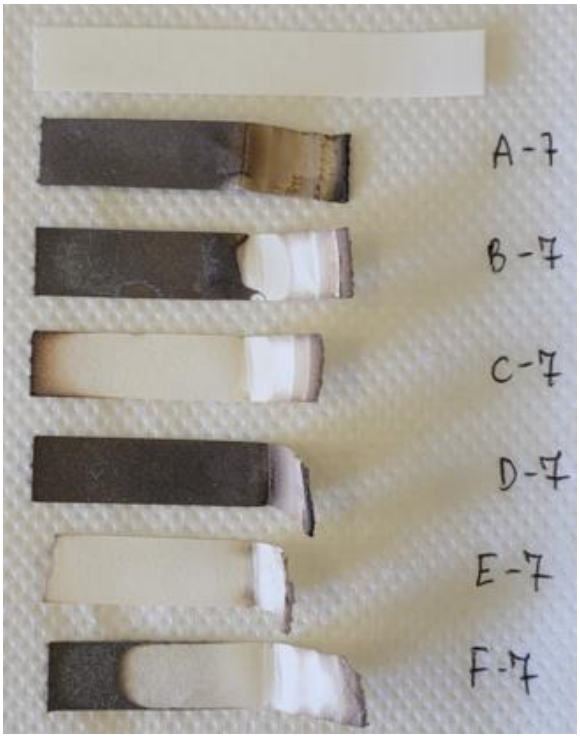

Figure S2. Pb-acetate strips recovered after seven days of incubation. A) BMM without As and Se oxyanions; B) 1 mM AsO_4^{3-}; C) 1 mM SeO_3^{2-}; D) 1 mM SeO_4^{2-}; E) 1 mM AsO_4^{3-} + 1 mM SeO_3^{2-}; F) 1 mM AsO_4^{3-} + 1 mM SeO_4^{2-}. The white paper on top is a blank of unused Pb-acetate paper.

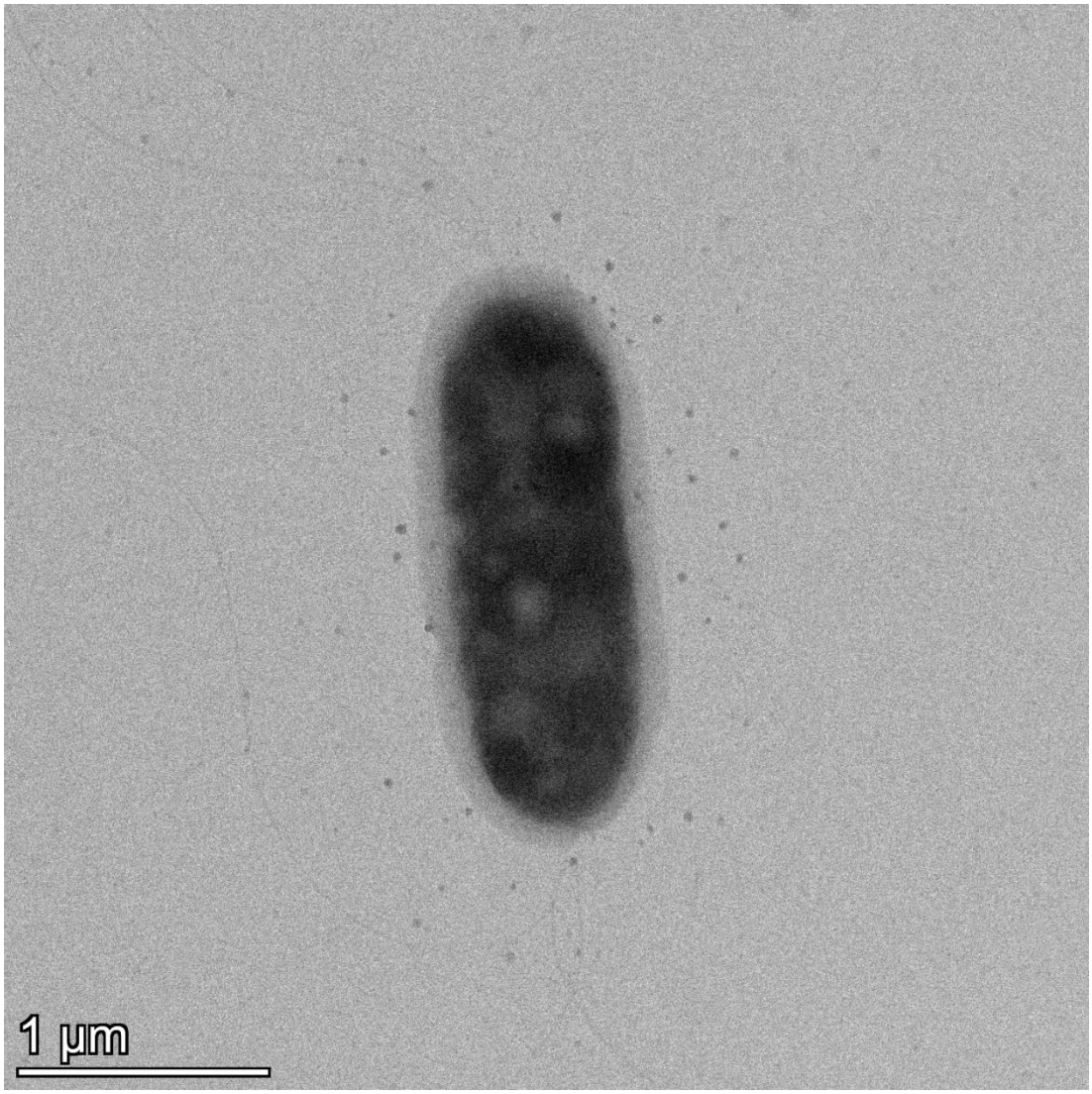

Figure S3. Bright-field TEM image of a cell of *Shewanella* sp. O23S from control incubation (bottle A). Extracellular polymeric substances (EPS) and flagella can be observed but no mineral deposits.

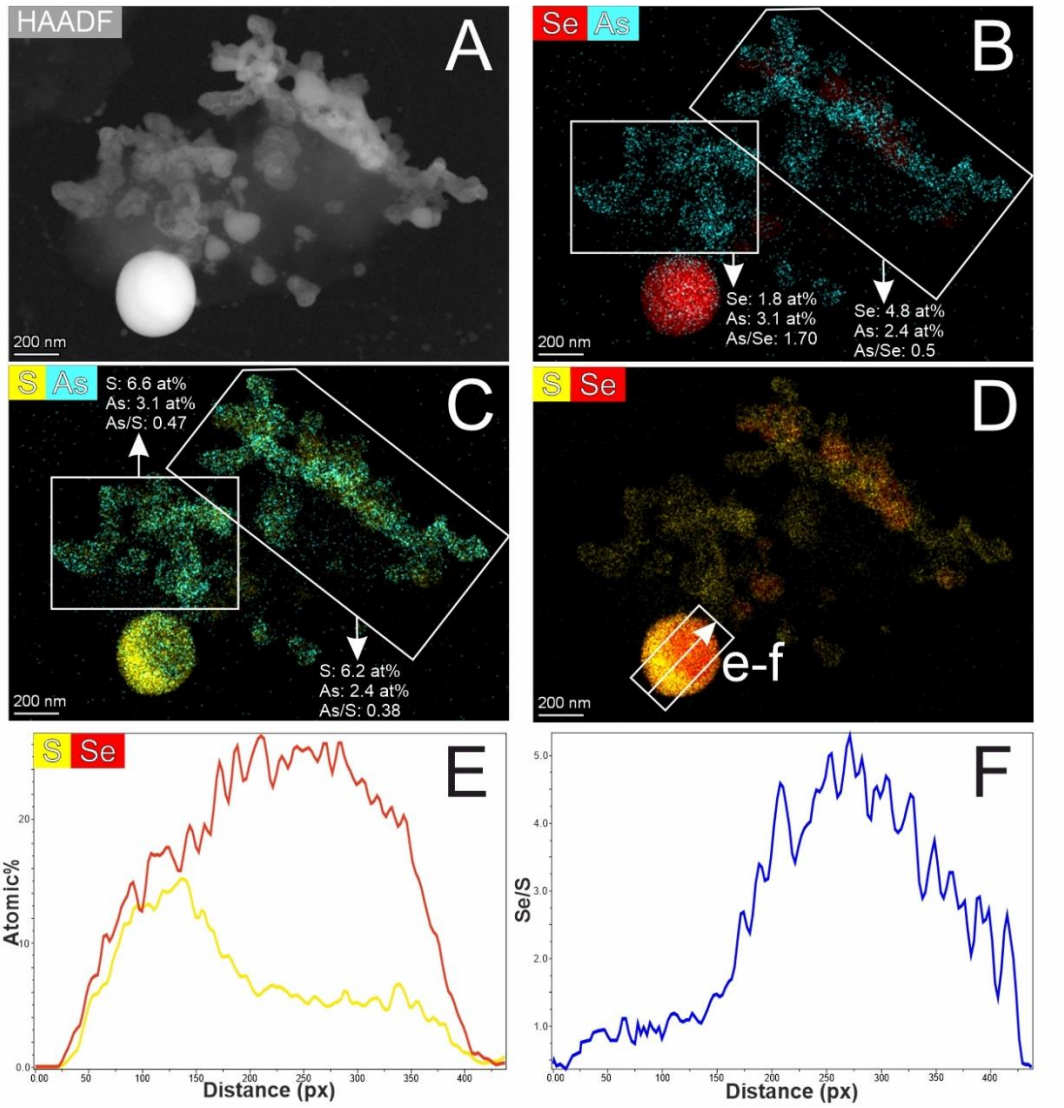

Figure S4. Elemental variability within the particles from the AsO_4^{3-} + SeO_4^{2-} incubations**.** A) STEM HAADF image of a cell with attached cloudy As-S aggregates and $Se(-S)^0$ nanoparticles, and B-D) corresponding EDS elemental maps with the calculated atomic percent (at%) and atomic ratios of the indicated areas. E) Variations of the concentrations of S and Se and F) the Se/S ratio within a single globular particle that consists primarily of Se with some S. The detected X-ray intensities within the white rectangle in D are integrated and calculated along the white arrow. (The indicated at% values should be interpreted with an understanding that in each analyzed area C, N and O are major components because of the contribution of the associated cell material and the amorphous C substrate of the TEM grid; however, since these elements are not present in the Se- and As-bearing biominerals, their concentrations are not shown)

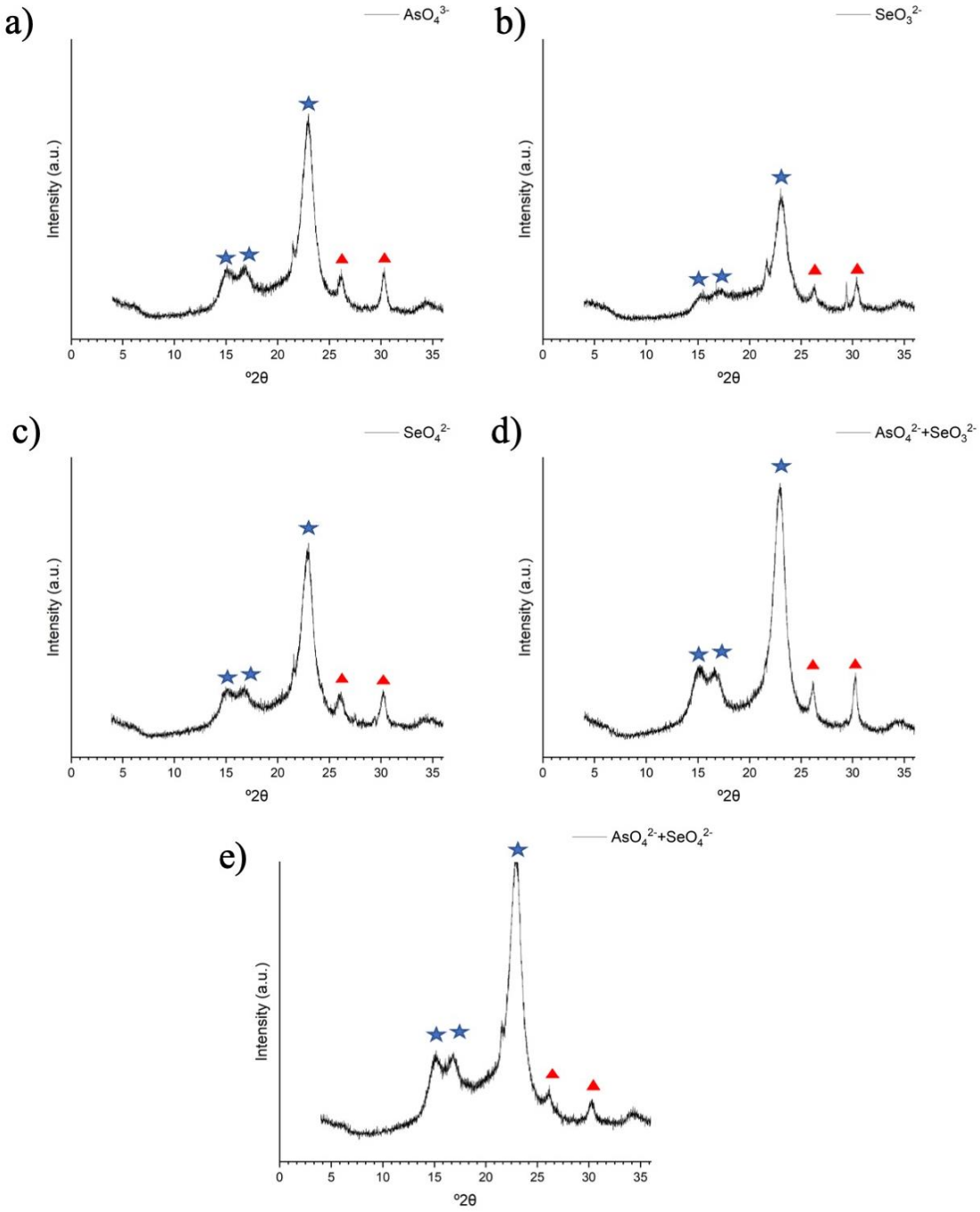

Figure S5. XRD patterns of lead acetate strips from incubations in BMM with added a) AsO_4^{3-}; b) SeO_3^{2-}; c) SeO_4^{2-}; d) AsO_4^{3-} and SeO_3^{2-}; and e) AsO_4^{3-} and SeO_4^{2-}. ★: diffraction peaks from lead acetate (ICDD code 00-054-0326) ▲: diffraction peaks from lead sulfide (galena) (ICDD code 01-078-1058).